Implementation of for Petrophysical interpretation of electrical measurements

[1]ANKITA MUHURI,
Gandhi Institute of Excellent Technocrats, Bhubaneswar, India
[2]SOLEKHA SWAIN,
Vivekananda Institute of Technology, Bhubaneswar, Odisha, India

ABSTRACT

Petrophysical interpretation of resistivity measurements is often hindered by the dependence of resistivity on the interconnected pore fluids and the interconnected pore surfaces. Induced polarization (IP) measurements yield parameters that are only controlled by the interconnected pore surfaces, thereby offering the opportunity to constrain interpretation of resistivity measurements. Using a database composed of 63 sandstone and unconsolidated sediment samples covering nine independent investigations, we identified a strong linear relationship between the real part of surface conductivity ($\sigma_{s\,urf}^{0}$) determined from multisalinity (σ_w) resistivity measurements and the imaginary conductivity (σ'') measured with IP at a frequency of about 1 Hz. We found $\sigma''/\sigma_{s\,urf}^{0} \approx l \approx 0.042$ with a coefficient of determination (R^2) of 0.911 and a standard deviation of l of 0.022. We found a similar relation when the normalized chargeability (from Debye decomposition) of the frequency dependence of the IP response is used instead of $\sigma 0$. By estimating the true formation factor (F) recorded at high salinity, we solved for $\sigma_{s\,urf}^{0}\delta\sigma_w\text{Þ}$ and found that it parallels the salinity dependency of the imaginary conductivity, $\sigma''\delta\sigma_w\text{Þ}$, as reported in recent studies. We also found that the value of the l determined from this experimental study was generally consistent with predictions of the POLARIS model when the mobility of the ions in the Stern layer was assumed to be $1/350$ of the mobility of the ions in the diffuse layer (considered equal to the mobility of the ions in the bulk solution). We discovered how the identified relationship can be used to significantly improve (1) the estimation of the true formation factor and (2) the groundwater conductivity, from a single salinity resistivity measurement when an IP measurement is also made. The approach offers an opportunity to improve estimation of porosity, formation factor, and salinity in well logging and hydrogeophysical investigations.

INTRODUCTION

The petrophysical interpretation of resistivity data is inherently uncertain due to the competing properties of the pore fluids, pore geometry, and pore surface area on resistivity measurements. Electrical resistivity of a porous medium depends on the chemical composition of the pore fluids, the temperature, the volumes of the conducting and nonconducting saturating fluids, the interconnected porosity and tortuosity of the pore network, and the surface area of the interconnected pore network. Consequently, reliable estimation of lithological properties from resistivity measurements usually requires external supporting data sets to constrain some of the properties controlling resistivity. A common problem with the interpretation of resistivity data is quantification of the extent to which electrolytic conduction through the connected pore network, versus surface (interfacial) conduction along the interconnected mineral-fluid interface, controls resistivity. This problem often complicates lithologic interpretation from resistivity well logs. For example, resistivity well logs are often used to estimate porosity from the electrical formation factor when it is assumed that the conductivity of the pore fluids is high enough such that surface conduction is insignificant relative to electrolytic conduction. This assumption is often not valid, and it is historically well known to cause inaccuracy in the calculation of the true formation factor and/or the rock porosity.

Additional geophysical information may help limit the uncertainty in the petrophysical interpretation of resistivity measurements.

Induced polarization (IP) measurements may be particularly valuable in this respect as additional information beyond the resistivity

magnitude is obtained; a measure of charge storage (polarization) relative to electromigration is simultaneously acquired. It is well recognized that IP measurements are primarily controlled by the lithological properties of the rock and are weakly, relative to resistivity measure- ments, controlled by the pore-fluid composition. More specifically, IP measurements directly sense the polarization of the mineral-fluid in- terface and are primarily related to the surface area of the intercon- nected pore network. Electrical models for the complex conductivity of a rock often represent the surface conductivity as a complex term, where the real part of the surface conductivity represents electromi- gration of charge along the mineral-fluid interface sensed with a resistivity measurement, and the imaginary part represents the polari- zation of charge at the mineral-fluid interface as sensed with an IP measurement. Assuming that the real and imaginary parts of the sur- face conductivity are related, the opportunity to reduce ambiguity in petrophysical interpretation of resistivity measurements by making an IP measurement therefore exists.

This opportunity to improve interpretation of resistivity data sets using IP measurements has been recognized and previously demonstrated in a qualitative sense (Slater and Lesmes, 2002). However, petrophysical relations for resistivity constrained by information on IP are unavailable. This is a consequence of the fact that a quantitative relationship between surface conductivity sensed with a resistivity measurement and interfacial polarization sensed with IP is lacking. Some limited work has been performed to determine the form of this relationship, but studies have been focused on a narrow range of samples (e.g., Börner, 1992; Börner et al., 1996). For example, Revil and Skold (2011) only note that the salinity dependence of the surface conductivity and quadrature conductivity "seems to be the same" for a single sample from the Börner (1992) study. The establishment of a robust quantitative relationship between surface conductivity and common IP parameters could significantly advance the reliability of the petrophysical information (e.g., formation factor, porosity, permeability, and pore-fluid salinity) obtained from IP measurements.

Motivated by this opportunity, our objective was to assemble an extensive database to experimentally determine the relationship between surface conductivity and IP measurements. As we shall show, establishing this relationship requires accurate measurements of the complex conductivity over a wide enough salinity range that the real part of the surface conductivity can be reliably quantified. Here, we report on an extensive database of samples that has been compiled and interpreted to investigate this relationship. We also demonstrate how this relationship can be used to improve the reliability of the interpretation of petrophysical parameters (formation factor and water conductivity) from single salinity resistivity and IP measurements. Finally, we examine how our experimental observations are consistent with recently proposed mechanistic model for the complex conductivity of shaly sands (Revil, 2012).

ELECTRICAL PROPERTIES

Measurements

The electrical conductivity of rocks, which includes conduction and polarization effects, can generally be represented by a complex quantity σ^{ω}, which is expressed in terms of magnitude $|\sigma|$ and phase

$$\sigma^{\omega} = |\sigma| e^{i\varphi} = \sigma' + i\sigma''$$

with $i = \sqrt{-1}$ being the imaginary unit. Generally, the complex electrical conductivity of earth materials is frequency dependent $\sigma^{\omega}(\omega)$, where the angular frequency (ω) is related to the measured frequency (f) by $\omega = 2\pi f$. The spectrum of complex conductivity $\sigma^{\omega}(\omega)$ contains information on the electrical properties of the sample over the investigated frequency interval. Whereas the real or in-phase component of conductivity $\sigma'(\omega)$ represents current flow via electromigration, the imaginary or quadrature component of conductivity $\sigma''(\omega)$ represents polarization phenomena (e.g., Vinegar and Waxman, 1984).

Spectral IP (SIP) measurements provide additional information than what is obtained from a single frequency measurement of conductivity. SIP measurements are typically made over a frequency range from as low as 10^{-3} to 10^{3} Hz. Relaxation models can be used to concisely represent the shape of the complex conductivity dependence on frequency in terms of a small number of parameters. Nordsiek and Weller (2008) introduce a Debye decomposition (DD) approach to concisely represent the measured frequency-dependent complex conductivity of a sample. In this approach, $\sigma^{\omega}(\omega)$ is represented by a superposition of Debye relaxation models,

$$\sigma^{\omega}(\omega) = \sigma_0 \left(1 - \sum_{j=1}^{n} m_j \left(1 - \frac{1}{1 + i\omega\tau_j}\right)\right); \qquad (2)$$

with m_j and τ_j being, respectively, the chargeability and relaxation time parameters of a single relaxation term.

Decomposition of the spectra into several Debye models results in a distribution of relaxation times that can be concisely summarized by four integrating parameters. The first parameter is the conductivity σ_0 obtained from extrapolation of the amplitude spectra to low frequency.

According to the original definition of chargeability (m) given, for example, by Sumner (1976),

$$m = \frac{\sigma_{\infty} - \sigma_0}{\sigma_{\infty}}; \qquad (3)$$

φ or by real (σ') and imaginary (σ'') components,

where σ_∞ is the high-frequency asymptotic value. The chargeability therefore quantifies the relative change of conductivity in a frequency scan. The polarization magnitude m_j computed for each individual Debye relaxation term therefore specifies the conduc- tivity change over a narrow frequency interval. The summation across the measured frequency range yields a global polarization magnitude term, defined here as total chargeability,

$$m_t = \sum_{j=1}^{n} m_j; \quad (4)$$

being the second integrating parameter of a DD. The multiplication of total chargeability m_t and low-frequency conductivity σ_0 gives the normalized chargeability,

$$m_n = m_t \sigma_0: \quad (5)$$

The normalized chargeability m_n represents a global polarization magnitude similar to imaginary conductivity except that it is weighted by the observed frequency dependence. The third and

fourth integrating parameters of the DD are the mean relaxation time and the degree of uniformity. For the sake of brevity, these parameters are not defined here as they are not used in our analysis.

Models

Most models for the complex electrical conductivity of a porous material at low frequencies (e.g., less than 100 Hz) are based on a parallel addition of two conduction terms representing (1) an electrolytic contribution via conduction through the interconnected pore space (σ_{el}) and (2) a mineral surface conduction contribution (σ''_{surf}) (e.g., Vinegar and Waxman, 1984),

$$\sigma'' = \sigma_{el} + \sigma''_{surf}; \tag{6}$$

Polarization is only associated with the surface conductivity at low frequencies. For a fully saturated medium,

$$\sigma' = \frac{1}{F}\sigma_w + \sigma'_{surf}; \tag{7}$$

and

$$\sigma'' = \sigma''_{surf}; \tag{8}$$

where F is the electrical formation factor and σ_w is the fluid conductivity.

Archie's law is commonly used to represent F in terms of the interconnected porosity (ϕ),

$$F = \phi^{-m}; \tag{9}$$

where m is the cementation exponent.

Empirical and mechanistic formulations for the surface conductivity exist but are not as well established as Archie's classic law. These formulations describe the surface conductivity in terms of (1) the volume-normalized surface area or the cation exchange capacity and (2) factors such as the surface charge density and surface charge mobility (Waxman and Smits, 1968; Rink and Schopper, 1974; Vinegar and Waxman, 1984; Revil and Skold, 2011). We consider the formulation of one recent mechanistic model in detail below.

Understanding the controls on the electromigration component of the complex surface conductivity has been in part limited by the fact that laborious multisalinity measurements are required to estimate σ'_{surf}. This is most commonly achieved by fitting the linear relation shown in equation 7 to multisalinity measurements of σ' and assuming a salinity-independent σ'_{surf} (Revil, 2012). In this paper, we describe an alternative approach to estimate a salinity-dependent σ'_{surf}.

It is logical to assume that a relationship between the electromigration and polarization contributions to the complex surface conductivity will exist. Numerous studies have demonstrated how σ'' is primarily controlled by the pore volume-normalized internal surface area (e.g., Börner et al., 1996; Weller et al., 2010) or cation exchange capacity (Vinegar and Waxman, 1984; Revil, 2012). The polarization component of the complex surface conductivity can be directly defined by the measured imaginary conductivity

$$l = \frac{\sigma''_{surf}}{\sigma'_{surf}}; \tag{10}$$

was nearly independent of salinity for sandstone samples, but varied slightly with type of sandstone. Börner et al. (1996) report a variation of l between 0.01 and 0.15. However, dedicated experiments to better constrain the form of the relationship between σ'_{surf} and σ''_{surf} are lacking.

Salinity independence is often implicitly assumed in the estimation of σ'_{surf}. Rink and Schopper (1974) propose a salinity-dependent surface conductivity, and the salinity dependence of surface conductivity has been theoretically treated through merging a surface complexation model with electrical double-layer theory (Revil and Glover, 1997; Leroy and Revil, 2004). Estimation of σ'_{surf} from measurements of σ' as a function of σ_w yields a salinity-independent σ'_{surf} estimate (equation 7). However, σ'' depends on fluid chemistry (Lesmes and Frye, 2001; Weller et al., 2011), with models attributing the salinity dependence to variations in the surface charge density, counterion mobility, and pH (Börner, 1992; Revil and Skold, 2011; Skold et al., 2011). These models predict an asymptotic behavior, with σ'' reaching a constant maximum value at high salinity. However, experimental observations also suggest a dependence of σ'' on variations in the surface ionic charge mobility with salinity change (Lesmes and Frye, 2001; Weller and Slater, 2012), causing a σ'' decrease at the highest salinities. Such dependence has yet to be incorporated into models. Assuming that σ'_{surf} and σ'' are indeed closely related, a salinity dependence of σ'_{surf} is expected.

Theoretical considerations: Assessment from the POLARIS model

Revil (2012) introduces the POLARIS model to describe the complex conductivity of (pyrite-free) shaly poorly sorted sands. This model invokes the effective medium theory for grains coated by an electrical double layer and immersed in a background electrolyte. The model assumes that the polarization is primarily attributed to the discontinuous Stern layer around individual grains, whereas the electromigration is primarily associated with the interconnected diffuse layer. The real part of the surface conductivity in the POLARIS model is defined as

$$\sigma'_{surf} = m\,\frac{F-1}{F}\,\frac{2}{3}\,\frac{\phi}{1-\phi}\,\beta_S\,Q_v; \tag{11}$$

where Q_V represents the excess surface charge and β_S represents the effective surface mobility in the electrical double layer. Equation 11 is considered valid when the Dukhin number (Dukhin and Shilov, 2002), representing the ratio of the in-phase surface conductivity of the grains to the electrical conductivity of the pore water, is much less than 1.

In the POLARIS model, the effective surface mobility of the electrical double layer is attributed to ions in the Stern layer and the diffuse layer,

$$\beta_S = \beta_{Stern} f + \beta_{diff}(1-f); \tag{12}$$

(equation 8). Börner (1992) finds that the ratio of the two surface conductivity components,

where $\beta^{S}_{\text{counterions}}$ is the mobility of the counterions in the Stern layer, β_{cations} is the mobility of the cations in the pore water (or in the diffuse

layer), and f is the partition coefficient. Whereas the mobility of cations in pore water is well known, the mobility of ions in the Stern layer is less certain. The value of $\beta_{\delta b p}$ is well known, being 5.2 × 10^{-8} $m^2/\delta sV\flat$ for sodium cations at 25 °C. Previous work on SIP model development has for simplicity assumed that $\beta^S_{\delta b p}$ is approximately equal to $\beta_{\delta b p}$ (Revil and Florsch, 2010). However, in his POLARIS model, Revil (2012) finds from observations $\beta^S_{\delta b p} \frac{1}{4}$ 1.5×10^{-10} $m^2/\delta sV\flat$ for sodium cations at 25 °C, such that $\beta^S_{\delta b p}/\beta_{\delta b p} 0 1 \delta 0029$, suggesting that the mobility of the counterions in the Stern layer is considerably lower than in the pore water or diffusive layer. The partition coefficient (f) denotes the fraction of counterions in the Stern layer relative to the total surface concentration of counterions in the Stern and diffuse layer combined. The coefficient is salinity dependent and controlled by the type of clay minerals that are dominant, with f being smaller for swelling clays such as smectite than for nonswelling clays such as illite and kaolinite, where $f > 0.95$ (Leroy and Revil, 2009).

The imaginary conductivity in the POLARIS model is defined as

$$\sigma'' \frac{1}{4} \frac{F-1}{F} \frac{2}{3} \frac{\phi}{\phi-1} \beta^S_{\delta b p} f Q_V; \quad (13)$$

and it only includes a contribution from the Stern layer.

Using equations 11-13, the ratio of the imaginary conductivity to the real part of the surface conductivity is given by

$$l \frac{1}{4} \frac{\sigma 0}{\cap\ surf} \frac{1}{4} \frac{\beta^S_{\delta b p} f}{m \beta^S_{\delta b p} f \flat \beta_{\delta b p} \delta 1 - f \flat}; \quad (14)$$

i.e., l only depends on the cementation factor m, the partition coefficient f, and the cation mobilities $\beta^S_{\delta b p}$ and $\beta_{\delta b p}$. Assuming that

$$\beta^S_{\delta b p}/\beta_{\delta b p} < \delta 1 - f \flat / f; \quad (15)$$

equation 14 simplifies to

$$l \frac{1}{4} \sigma'' \frac{}{\sigma^0_{s\ urf}} \cong \frac{1}{m} \frac{\beta^S_{\delta b p}}{\beta \delta b p} \frac{f}{1-f} :; \quad (16)$$

It should be noted that Revil (2012) shows in his Figure 8 a similar linear relation between scaled surface conductivity $\sigma^0_{s\ urf} \delta f_M / \delta 1 - f_M \flat \flat$ and the imaginary part of conductivity with f_M being the maximum partition coefficient reached at high salinity. He identified from the slope of the linear relation a mobility ratio $\beta^S_{\delta b p}/\beta_{\delta b p} 0 \frac{1}{4} 00148$. Considering that the slope predicted by equation 16 is the mobility ratio divided by the cementation factor m, the mobility ratio should be multiplied by m to get a better approximation. Assuming an average $m \approx 2$, we get the mobility ratio used above.

METHODS

Our database is made up of 63 samples with $\sigma^{\omega} \delta \omega \flat$ recorded as a function of salinity compiled from multiple sources (Flath, 1989; Börner, 1992; Lesmes and Frye, 2001; Breede, 2006; Kruschwitz, 2008; Schröder, 2008; Revil et al., 2013) and hitherto unpublished studies. The database is summarized in Table 1, which shows the salinity range (mS/m) over which $\sigma^{\omega} \delta \omega \flat$ was recorded, the number also shown where known. All samples were saturated with NaCl solution. As pH values are unavailable, we assume near neutral conditions, i.e., well above the point of zero charge (pH of approximately 3 for silica). Although our understanding is not yet complete, the pH appears to exert a weak dependence on surface conductivity (Lesmes and Frye, 2001; Revil et al., 2013).

All measurements reported in Table 1 were obtained by measuring the impedance magnitude and phase shift of the voltage waveform recorded across the sample relative to the current waveform recorded on a reference resistor, the source typically being a sine signal (e.g., Slater and Lesmes, 2002). All measurements reported here were recorded using a four-electrode device, whereby separate electrode pairs were used to inject the current into the sample and record the resulting potential waveform across the sample. Measured magnitude and phase were converted into a measured complex conductivity (σ^{ω}) using the geometric factor defining the measurement geometry and the resulting current flow path in the test device.

Equation 7 can be directly used to estimate F and $\sigma^0_{\ surf}$ from the measurements of σ^0 versus σ_w. However, this approach yields a single (salinity independent) $\sigma^0_{s\ urf}$ estimate, whereas we expect $\sigma^0_{s\ urf}$ to depend on salinity. A salinity-dependent surface conductivity $\sigma^0_{s\ urf} \delta \sigma_w \flat$ can be estimated if the salinity range extends to a high enough salinity that $\sigma_w \gg \sigma^0_{s\ urf}$ then,

$$\sigma^0 \cong \frac{1}{F} \sigma_w :; \quad (17)$$

Assuming the salinity range is high enough, the true formation factor retrieved from equation 17 can be used to determine a salinity-dependent surface conductivity:

$$\sigma^0_{s\ urf} \delta \sigma_w \flat \frac{1}{4} \sigma^0 \delta \sigma_w \flat - \frac{1}{F} \sigma_w :; \quad (18)$$

This approach was adopted in this study.

Some of our samples were acquired over a limited salinity range, where the approximation shown in equation 17 may not be valid. If surface conductivity remains significant, then an apparent formation factor F^0 determined from equation 17 will increase as salinity increases, until σ_w is sufficiently large such that the contribution of $\sigma^0_{s\ urf}$ to σ^0 becomes vanishingly small (e.g., Lesmes and Frye, 2001).

For most samples of our study, the true formation factor was determined from the high-salinity slope of the function $\sigma^0 \delta \sigma_w \flat$. The of salinities, and a description of the sample. The sample porosity is

inverse of this slope, computed from the largest salinities of the ex- periment, provides a reliable estimate of the true formation factor F (Flath, 1989). In the case of a limited salinity range, the true for- mation factor can be approximated from fitting the expected asymp- totic behavior of $F^0\ \sigma_w$ versus σ_w because F^0 should approach a constant value ($F^0 \quad F$) at high salinities. This approach to estimat- ing F was applied to some sandstone samples and all unconsoli- dated samples of the database reported here. Figure 1 shows two example data sets in which measurements were fit to the relation

$$F^0 \quad \frac{F\sigma_w}{a \text{ þ } \sigma_w}\ ; \qquad (19)$$

where a is used as a free parameter that corresponds to the product $F\sigma^0_{\text{surf}}$. The apparent formation factor F^0ðσ$_w$Þ is determined from the

ð Þ
¼

¼

Table 1. Summary of the samples used in this study.

Sample	σ_w range (mS/m)	# salinities	Description	ϕ (-)	F (-)	σ' (mS/m)	σ'' (mS/m)	σ'_{sat} (mS/m)	I (-)	F' (-)	F_p (-)	m (-)	f (-)
1. Sandstones													
Flath (1989)													
H18H	24-9813	10	Triassic shaly sandstone	0.191	18.60	24.76	0.619	18.76	0.033	4.51	11.13	1.766	0.953
H18V	23-9851	10	Triassic shaly sandstone	0.199	17.10	25.58	0.635	19.09	0.033	4.34	10.61	1.759	0.953
H46H	112-9986	8	Triassic shaly sandstone	0.208	12.90	24.74	0.537	16.08	0.033	4.51	9.34	1.629	0.950
H46V	113-9966	8	Triassic shaly sandstone	0.218	11.50	24.55	0.512	14.70	0.035	4.61	9.15	1.603	0.951
H62H	112-1004	8	Triassic shaly sandstone	0.179	13.80	18.48	0.383	10.34	0.037	6.08	11.99	1.526	0.951
H62V	111-9937	8	Triassic shaly sandstone	0.183	14.80	17.87	0.400	10.37	0.039	6.21	13.30	1.587	0.955
HCF120H	23-10080	10	Triassic shaly sandstone	0.177	29.10	31.86	0.648	28.03	0.023	3.59	6.77	1.947	0.940
HCF120V	24-9803	10	Triassic shaly sandstone	0.170	44.10	23.74	0.465	21.20	0.022	4.72	8.85	2.137	0.942
HCF197H	112-10030	8	Triassic shaly sandstone	0.215	12.80	23.66	0.818	14.92	0.055	4.73	26.71	1.659	0.969
HCF197V	113-9918	8	Triassic shaly sandstone	0.213	11.80	20.81	0.682	11.22	0.061	5.44	24.75	1.596	0.971
HCF233H	23-9870	10	Triassic shaly sandstone	0.199	18.00	23.52	0.817	17.37	0.047	4.71	27.19	1.790	0.967
HCF233V	23-10020	10	Triassic shaly sandstone	0.177	28.10	22.45	0.731	18.53	0.039	4.92	21.90	1.926	0.963
HCF236H	24-9966	10	Triassic shaly sandstone	0.193	18.60	23.16	0.765	17.12	0.045	4.85	22.76	1.777	0.965
HCF236V	23-9736	10	Triassic shaly sandstone	0.208	17.70	20.18	0.708	13.87	0.051	5.53	33.66	1.830	0.970
P19H	23-9851	9	Triassic shaly sandstone	0.213	13.30	21.31	0.789	12.83	0.061	5.29	44.62	1.673	0.973
P19V1	24-9985	9	Triassic shaly sandstone	0.219	12.90	21.17	0.806	12.34	0.065	5.38	57.73	1.684	0.974
P39H1	112-9966	8	Triassic shaly sandstone	0.219	13.00	29.31	0.934	20.72	0.045	3.81	15.80	1.689	0.964
P39V1	111-9966	8	Triassic shaly sandstone	0.226	12.10	23.82	0.875	14.63	0.060	4.67	37.19	1.676	0.972
P40H1	24-9851	9	Triassic shaly sandstone	0.213	15.90	29.11	1.026	22.06	0.047	3.85	23.94	1.789	0.967
P40V1	24-9909	9	Triassic shaly sandstone	0.216	17.40	24.57	1.006	18.04	0.056	4.62	180.25	1.864	0.973
P53H1	23-9793	9	Triassic shaly sandstone	0.233	11.90	43.56	0.978	34.18	0.029	2.56	5.51	1.700	0.944
P56V	23-9765	9	Triassic shaly sandstone	0.221	15.70	42.60	0.761	35.52	0.021	2.61	4.54	1.824	0.931
P68H1	23-9659	9	Triassic shaly sandstone	0.218	15.90	33.04	0.986	25.95	0.038	3.41	11.79	1.816	0.960
P68V	23-9640	9	Triassic shaly sandstone	0.225	13.10	35.36	1.073	26.67	0.040	3.22	11.60	1.725	0.960
Börner (1992)													
E10	2.9-5100	7	Elbe sandstone	0.224	16.40	18.50	0.275	12.88	0.021	4.98	7.71	1.870	0.937
E12	3.1-5110	8	Elbe sandstone	0.259	10.99	9.09	0.061	0.88	0.069	9.92	11.81	1.774	0.977
B2	3.2-5340	6	Bentheim sandstone	0.194	15.58	15.70	0.018	0.36	0.050	15.22	15.65	1.674	0.967
F3	1.6-1600	6	Fontainbleau sandstone	0.068	115.32	0.72	0.002	0.07	0.028	104.59	111.38	1.766	0.944
Tezuka and Frye (2001)													
B_LF	22-7800	5	Berea sandstone	0.189	16.70	10.48	0.088	2.80	0.031	12.35	15.58	1.615	0.917
Breede (2006)													
GR	6.7-8988	13	Glauconitic sandstone	0.246	11.66	12.64	0.291	4.75	0.061	7.28	16.11	1.751	0.974
BU3	7.8-2310	10	silty Bunter sandstone	0.089	68.35	4.51	0.180	3.17	0.057	20.32	389.92	1.746	0.972
BU12	7.2-2188	10	Bunter sandstone	0.181	17.64	6.00	0.054	0.54	0.099	16.05	20.39	1.679	0.983
BK	7.4-2242	10	Helsby formation	0.160	18.22	6.39	0.043	1.13	0.038	15.01	17.86	1.584	0.954
BS4	7.4-2242	10	Kidderminster formation	0.166	17.84	8.04	0.161	2.35	0.069	12.62	24.18	1.605	0.974
BR5	6.7-2232	9	Helsby formation	0.243	9.04	12.57	0.271	2.05	0.132	7.55	15.55	1.596	0.969
Schröder (2008)													
BU1	25-2150	8	Bunter sandstone	0.140	38.03	9.32	0.334	6.95	0.048	9.66	66.40	1.796	0.969
OK4	25-2150	8	Oberkirchen sandstone	0.180	24.77	6.33	0.112	2.69	0.042	14.23	24.64	1.872	0.964
GR1	25-2150	8	Glauconitic sandstone	0.240	9.41	13.26	0.293	3.70	0.079	6.79	14.33	1.571	0.977
B49H	25-630	6	Bahariya formation	0.180	26.82	3.85	0.029	0.49	0.080	23.90	28.62	1.795	0.974
B49V	25-631	6	Bahariya formation	0.160	30.98	3.61	0.029	0.71	0.042	24.90	30.91	1.874	0.964
B4H	25-632	6	Bahariya formation	0.120	44.94	2.70	0.054	0.69	0.078	33.37	63.60	1.795	0.980
B4V	25-633	6	Bahariya formation	0.130	59.56	2.37	0.039	0.86	0.045	38.01	62.32	2.003	0.969
Kruschwitz (2008)													
B	36-775	9	Baumberg sandstone	0.191	12.84	21.91	0.341	15.02	0.055	4.04	6.41	1.515	0.951
C	36-775	9	Cotta sandstone	0.217	12.53	18.81	0.374	11.75	0.032	4.70	8.92	1.654	0.948
2. Unconsolidated sediments													
Revil et al. (2013)													
S9	38-2333	5	saprolite	0.480	4.10	36.30	0.661	6.79	0.097	3.33	5.88	1.922	0.985
S16	39-2350	5	saprolite	0.490	5.90	30.70	0.796	10.19	0.078	3.94	10.30	2.488	0.985
S22	40-2349	5	saprolite	0.430	4.40	67.30	1.630	39.57	0.041	1.81	4.28	1.756	0.962
New data													
B1_47.65-49	3-300	6	Sands and gravels	0.170	12.53	9.12	0.015	1.14	0.013	10.97	11.41	1.427	0.885
B2,4, 35-36.45	3-300	6	Sands and gravels	0.154	9.50	10.94	0.008	0.41	0.020	9.14	9.30	1.203	0.892
B3_2_14.8-16	3-300	6	Sands and gravels	0.122	12.29	8.71	0.017	0.57	0.029	11.48	12.03	1.192	0.924
B4_7_54-55.2	3-300	6	Sands and gravels	0.197	10.49	10.48	0.021	0.95	0.022	9.54	10.02	1.447	0.917
B6_2_52.95-54	4.2-300	6	Sands and gravels	0.144	13.01	8.53	0.034	0.85	0.040	11.72	12.95	1.324	0.949
C1_5_43.95-45	3.8-300	6	Sands and gravels	0.178	12.77	8.92	0.024	1.09	0.022	11.21	11.96	1.476	0.917
C2_7_52-53.8	3-300	6	Sands and gravels	0.164	14.62	7.54	0.015	0.70	0.022	13.27	13.94	1.484	0.919
C3_5_34.45-36	3-300	6	Sands and gravels	0.170	13.92	7.62	0.015	0.44	0.035	13.12	13.78	1.486	0.947
C3_3_17.05-18	3-300	6	Sands and gravels	0.219	8.20	12.89	0.019	0.69	0.027	7.76	8.03	1.385	0.928
C4_2_10.25-12.0	3-300	6	Sands and gravels	0.351	4.90	21.25	0.037	0.84	0.045	4.70	4.91	1.518	0.959
C5_5_34-46	3-300	6	Sands and gravels	0.169	10.65	10.17	0.018	0.78	0.024	9.83	10.28	1.330	0.916
LI-1	1.5- 95	8	Poorly sorted silty agricultural soil	0.377	6.37	16.10	0.026	1.13	0.023	5.92	6.16	1.897	0.939
LI-2	1.6- 95	7	Poorly sorted silty agricultural soil	0.377	9.31	11.77	0.016	1.55	0.010	8.08	8.35	2.287	0.890
2_21c47_48	15-119	6	Sand and gravel flood deposits		12.59	11.80	0.048	2.35	0.021	10.08	11.17		
2_19c50_51	20-371	7	Sand and gravel flood deposits		9.05	12.23	0.050	2.52	0.020	7.18	7.95		
2_24c42_43	14-109	6	Sand and gravel flood deposits		9.94	12.03	0.049	1.07	0.046	9.05	10.04		

slope of the curve $\sigma'(\sigma_w)$ over a certain range of σ_w. Considering the data of the Berea sandstone sample in Figure 1a, this procedure results in $F = 16.7$, which is slightly higher than the value of 15.9 reported in Lesmes and Frye (2001). Figure 1b displays the curve $F(\sigma_w)$ of the unconsolidated sand and gravel sample B3_2_14.8-16, where the maximum σ_w is 300 mS/m. The extrapolation according to equation 19 results in a true formation factor of 12.23. Only data sets in which F could be confidently estimated from this approach are included in Table 1.

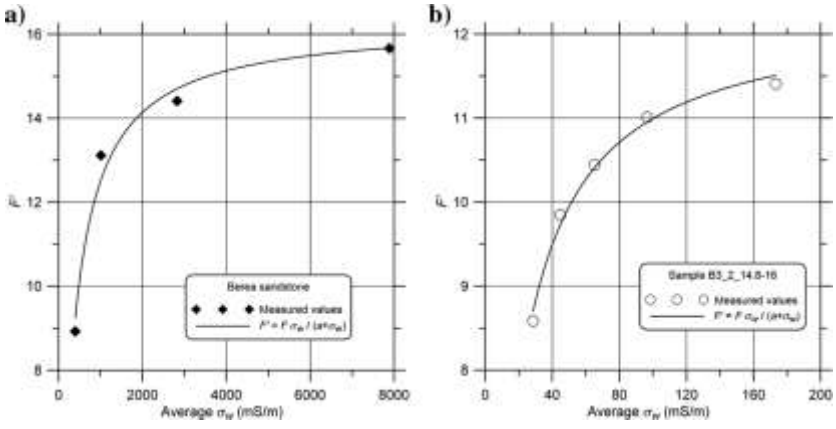

Figure 1. Procedure used to estimate true formation factor (F) from multisalinity measurements of the real conductivity. The apparent formation factor $F = \Delta\sigma_w/\Delta\sigma'$ determined from the inverse of local slope of $\sigma'(\sigma_w)$ versus σ_w is fit to equation 19, where F is given by the high-salinity asymptote: (a) example Berea sandstone and (b) example unconsolidated sediment.

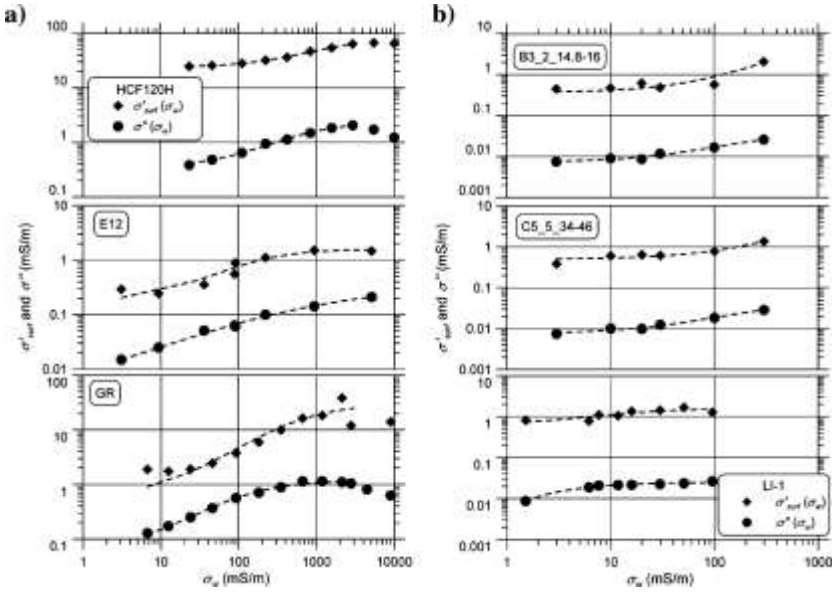

Figure 2. Examples of the dependence of $\sigma'_{s\,surf}$ and σ'' on salinity (σ_w). The fit of the data to the SLP model according to equation 20 is indicated: (a) selected sandstone samples and (b) selected unconsolidated samples. The SLP model is not shown at high salinity where $\sigma'_{s\,surf}$ or σ'' decrease with σ_w because such behavior is not predicted by the model

RESULTS

Results of the analysis of the 63 samples in our database are compiled in Table 1. We show the true formation factor F, the apparent formation factor computed at $\sigma_w \approx 100$ mS/m for each sample, $\sigma'_{s\,surf}$, and σ'' at $\sigma_w \approx 100$ mS/m. The conductivity values in Table 1 and the following figures correspond to a frequency of around 1 Hz. The samples span approximately three orders of magnitude of variation in $\sigma'_{s\,surf}$ (0.067 − 39.6 mS/m) and σ'' (0.0018 − 1.63 mS/m) at $\sigma_w \approx 100$ mS/m, illustrating that the database is well suited for this study. The true formation factor also varies widely, from 4.1 to 115, reflecting the range of samples from coarse unconsolidated sediments to cemented sandstones. Also shown in Table 1 are estimated values of l, m (estimated from equation 9, using porosity when available), and the partition coefficient (f) from equation 16 assuming a fixed ratio of mobilities $\beta_s/\beta_{fl} = 0.0029$ (Revil, 2012).

Figure 2 shows the salinity dependence of $\sigma'_{s\,surf}$ and σ'' for selected samples from our database. Figure 2a shows the sandstone samples HCF120H (Flath, 1989), ES12 (Börner, 1992), and GR (Breede, 2006). These samples were selected as measurements were recorded over a wide salinity range. The unconsolidated sand and gravel samples (B2_2_14.8-16, C5_5_34-46) and the agricultural soil (LI-1), which are shown in Figure 2b, were investigated at lower salinity. The imaginary conductivity shows the salinity dependence discussed in recent studies (Revil and Skold, 2011; Weller and Slater, 2012), which can be well described by a weak power law dependence at low salinities, with a high salinity asymptote. Complex conductivity models attribute this behavior to result from the increase in surface charge density as σ_w increases (Revil and Skold, 2011). The fitting lines in Figure 2 represent the salinity dependence of the Stern layer polarization (SLP) model according to the function

$$\sigma''(\sigma_w) = c_s + a_s \frac{\sigma_w}{b_s + \sigma_w}; \qquad (20)$$

with the three fitting parameters a_s, b_s, and c_s. The physical significance of these three parameters, and their relation to a model proposed by Revil and Skold (2011), is discussed in Weller and Slater (2012).

Some data sets shown in Figure 2 exhibit evidence for a decrease in σ'' at the very highest salinities that is not predicted by existing models (the model curves are only shown for the salinity range where such behavior is not observed). Weller and Slater (2012) present strong evidence for decreases in σ'' at the high salinities, which they attribute to a reduction in surface ionic mobility due to charge packing on the mineral

surface.

The $\sigma_{s\,urf}^{0}$ dependence on σ_w largely parallels the σ'' dependence, and most curves are well described by equation 20. Some significant differences are apparent at the high and low salinities. At the highest salinities, the decreases in $\sigma_{s\,urf}^{0}$ are not as pronounced as decreases in σ'', with $\sigma_{s\,urf}^{0}$ more adhering to asymptotic behavior. At low salinities, some samples show a clear low $\sigma_{s\,urf}^{0}$ asymptote that is not well defined in the σ^{00} curves. However, a low-salinity asymptote is observed in the σ'' curves of other samples reported in Weller and Slater (2012). In the intermediate salinity range of 50 − 1000 mS/m, $\sigma_{s\,urf}^{0}$ ðσ$_w$Þ is directly proportional to σ''ðσ$_w$Þ.

Figure 3 shows the relationship between $\sigma_{s\,urf}^{0}$ and σ'' for all samples in the database for a $\sigma_w \approx 100$ mS/m. The data are very well explained by a single linear relationship with the gradient l ¼ 0.042 (coefficient of determination, R^2, of 0.911). Exact values of l for each sample are reported in Table 1. The standard deviation of l is 0.022. Figure 4 shows the equivalent relationship between m_n and $\sigma_{s\,urf}^{0}$. A strong linear relation is again observed, with the gradient equal to l_{mn} ¼ 0.20 (R^2 ¼ 0.907). The higher value for the gradient in Figure 4 is expected as m_n represents the total additive polarization across the measured frequency range.

The value of l obtained from this analysis can be compared against the expectations from the POLARIS model. Adopting the ratio $\beta_{ðþÞ}^{S}/\beta_{ðþÞ}$ ¼ 0.0029 as per Revil (2012), the condition expressed by equation 15 is fulfilled for f < 0.997. For the 63 samples of our study, the partition coefficient f was calculated by transformation of equation 16 using (1) the values of σ^{00} and $\sigma_{s\,urf}^{0}$ at a fluid conductivity of about 100 mS/m, (2) m determined from ϕ and F (from the multisalinity measurements), and (3) assuming $\beta_{ðþÞ}^{S}/\beta_{ðþÞ}$ ¼ 0.0029. It should be noted that this ratio is only valid for sodium cations in clayey material (Revil, 2012). Using this approach, the mean value of f was determined to be 0.953 with a standard deviation of 0.025. Thus, the POLARIS model is consistent with our observations.

We next consider whether variations in the ratio l and the partition coefficient f between the samples are related to the type of predominant clay minerals. Flath (1989) reports the portion of smectite in the grain size fraction <5 μm of her investigated set of sandstone samples. Samples H18, H46, and H62 are regarded as "smectite-poor" samples with a smectite fraction below 20% for the grain size <5 μm. For all other samples from the Flath database, the smectite content exceeds 50%. Figure 5 displays the relation between l and f for this set of sandstone samples. Generally, an increase in l is related to an increase in f. The smectite-poor samples are identified at intermediate values of l and f. The smectite-rich samples are separated into two clusters. Low values of l and f are observed for the samples HCF120, P56, and P53. All remaining samples belong to the cluster of high values of l and f. Consequently, the expectation that higher-smectite content results in a lower partition coefficient, as predicted by Leroy and Revil (2009), is not confirmed by the experimental data of our study.

IMPROVED PETROPHYSICAL INTERPRETATION: EXAMPLES

Formation factor estimation

Knowing the value of l provides opportunities to improve the petrophysical interpretation of electrical measurements. The inherent ambiguity of resistivity measurements results from the dependence of the measurement on the properties of the pore fluids, interconnected pore volumes, and interconnected pore surface. We next consider how estimation of physical properties from resistivity measurements can be improved using an IP measurement and a known, or assumed, value of l.

We first consider the estimation of the formation factor, of prime importance in numerous disciplines including hydrogeophysics and geophysical well logging. It is common practice to estimate F from measurements of σ^{0} and σ_w at a single salinity under the assumption that the salinity of the fluid is sufficiently high such that $\sigma_{s\,urf}^{0}$ is negligible; i.e., the approximation of equation 7 to equation 17 is valid. This assumption is desirable as multiple salinity

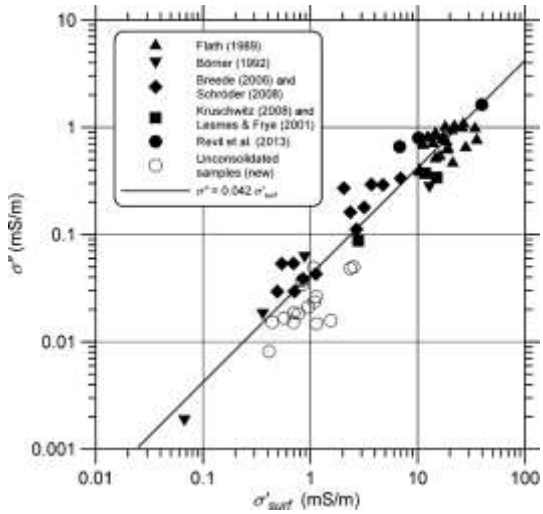

Figure 3. The dependence of imaginary conductivity (σ'') on surface conductivity ($\sigma_{s\,urf}^{0}$) for the entire database shown in Table 1. The value of σ'' at 1 Hz was used here. The best-fit line shows the single linear fit to the entire data set where l ¼ 0.042 with R^2 ¼ 0.911.

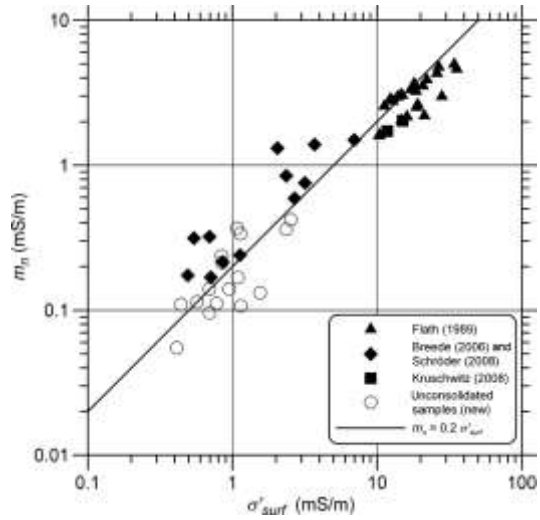

Figure 4. The dependence of normalized chargeability (m_n) on surface conductivity ($\sigma_{s\,urf}^{0}$) for 55 samples with available IP spectra. The best-fit line shows the single linear fit to the data set, where the mean ratio $m_n/\sigma_{s\,urf}^{0}$ ¼ 0.2 with R^2 ¼ 0.907.

measurements of electrical conductivity (σ^0 or σ_w) are often impractical in the field where only single-salinity data are available. Given an IP measurement, this assumption regarding σ^0_{surf} can be removed assuming l is known. According to Börner et al. (1996), a predicted value of the formation factor can be determined,

$$F_p = \frac{\sigma_w}{\sigma^0 - \sigma^0_{surf}} = \frac{\sigma_w}{\sigma^0 - \text{or}(\sigma''/l)}. \quad (21)$$

The potential for improved estimation of F was tested on our database. We compare the true formation factor (F) determined from multisalinity experiments via equation 19 and the asymptotic fitting procedure described above (1) to the apparent formation factor (F^0) estimated using a single salinity measurement via the common assumption that surface conductivity can be ignored (equation 17) and (2) with a predicted value of the true formation factor F_p estimated from the same single salinity measurement when incorporating information from IP using equation 21.

Figure 6 shows crossplots of F versus F^0 estimated for a single salinity electrical measurement at about 100 mS/m (Figure 6a) and F versus F_p (Figure 6b) considering σ'' from an IP measurement and an assumed constant value of l. Another option is to predict the formation factor using the normalized chargeabilty m_n, which is determined by DD from IP spectra. Equation 21 can be modified to

$$F_{p-mn} = \frac{\sigma_w}{\sigma^0 - \text{or}(m_n/l_{mn})}. \quad (22)$$

Figure 6c shows the crossplot F versus F_{p-mn}. In the case that surface conductivity is ignored (Figure 6a), the true formation factor is considerably larger than F^0 and never less than F^0. To quantify the

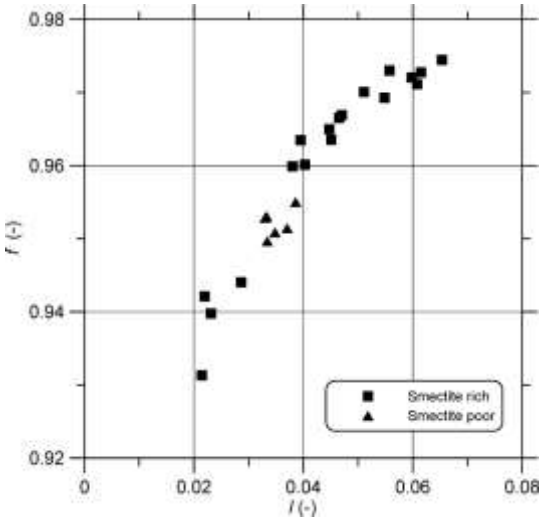

Figure 5. Relationship between estimated partition coefficient (f) and $l = \sigma''/\sigma^0_{surf}$ for sandstone samples from Flath (1989) in which smectite concentrations in the grain size fraction <5 μm are reported. The partition coefficient f was calculated by transformation of equation 16 using (1) the values of σ'' and σ^0_{surf} at a fluid conductivity of about 100 mS/m, (2) m determined from ϕ and F (from the multisalinity measurements), and (3) assuming $\beta^S_{\text{or}(p)}$.

difference between the true formation factor F and its predicted value F^{ω} (either F^0, F_p or F_{p-mn}), an average deviation (d) in logarithmic scale is defined by

$$d = \frac{1}{n} \times \sum_{j=1}^{n} |\log_{10}(F_j) - \log_{10}(F_j^{\omega})|. \quad (23)$$

Considering all 63 samples, the average deviation between F and F^0 as shown in Figure 6a reaches $d = 0.303$.

Figure 6b shows the result obtained using equation 21 and assuming a single value of $l = 0.042$ estimated for the entire database. The predicted formation factor (F_p) is now closer to the true formation factor (F) with an average deviation of only 0.174. Furthermore, data points are now scattered around the 1:1 line with some values of F_p larger than F. The systematic error caused by ignoring surface conductivity has been removed, and the remaining scatter results from the assumption of a single value of l (Figure 3) instead of using the individual value of l for each sample. The error bars indicate the downward variation of the predicted formation factor assuming a change in l within the interval between mean value and mean value plus standard deviation ($0.042 < l < 0.64$). The upward variation is not shown because equation 21 provides negative formation factors for some samples if l approaches 0.02 (mean value minus standard deviation). Figure 6c shows the result obtained using equation 22 and assuming a mean value of $l_{mn} = 0.20$ estimated for 55 samples with available IP spectra. The average deviation of the predicted formation factor F_{p-mn} is further reduced to $d = 0.126$.

Salinity estimation

We next consider the estimation of formation salinity (σ_w), also of high importance in well logging and hydrogeophysics. We use 12 sandstone samples from the database of Flath (1989) due to the wide range of salinities recorded. Furthermore, in such shaly sandstones, it is important to quantify surface conductivity to determine F and σ_w. Estimation of σ_w requires a known value of F. To simulate a well-logging situation, we estimate F based on equation 9 using a single value of $m = 1.75$, being the average value of these samples reported by Flath (1989), and the measured porosity. In a well-logging scenario, porosity could be measured using an independent technique (e.g., gamma-gamma).

Fluid conductivity was determined using equation 21 when (1) IP measurements were unavailable and surface conductivity was assumed to be negligible (i.e., $\sigma'' = 0$) and (2) when surface conductivity was estimated from σ'' and l (again set to 0.042). Figure 7 compares the two estimates against the known value of σ_w. The estimates are significantly improved when the IP data are included. An average deviation between predicted and true fluid conductivity is determined using an analogous equation to equation 23. Figure 8 displays the average deviation as a function of fluid conductivity. The average deviation considerably decreases with increasing fluid conductivity. Also in this case, the use of normalized chargeability instead of imaginary conductivity improves the predicting quality.

DISCUSSION

We have described a high-quality database of complex conductivity measurements spanning many different sample types

/βðþ ¼ 0.0029 (see text for further details).

and multiple independent studies. This database has permitted an

assessment of the dependence of σ_{surf}^{0} on salinity and the relationship between σ_{surf}^{0} and σ'' directly measured with IP. We have shown that σ_{surf}^{0} shows a characteristic salinity dependence that is comparable to the salinity dependence of the imaginary conductivity reported in recent studies (Revil and Skold, 2011; Skold et al., 2011; Weller et al., 2011; Weller and Slater, 2012; Revil et al., 2013).

Reliable estimation of the salinity-dependent surface conductivity was critically dependent on a robust estimate of the true formation factor (F). This follows from equation 18, where the accurate calculation of a small number from the subtraction of two large numbers is needed. Such a subtraction is only accurate when F is reliably determined. In samples that have a limited salinity range, we successfully estimated F through a fitting function that predicts a high-salinity asymptote for the salinity-dependent apparent formation factor (F^0).

We have presented experimental evidence for a single value of l, the ratio of the imaginary conductivity to the real part of the surface conductivity, representing a range of unconsolidated and consolidated samples, where σ_{surf}^{0} varies over three orders of magnitude. Based on 63 samples, we have reported a mean value of l ¼0.042, with a standard deviation of 0.022. The variation of l in our study between 0.01 and 0.13 (see Table 1) confirms the observation reported by Börner et al. (1996). Although there is significant scatter from the mean value (Figure 3), it is difficult to assign any significance to this deviation due to the above-mentioned uncertainties in the estimation of σ_{surf}^{0} from the direct subtraction of equation 18. These deviations may just represent the uncertainty in the computation of the true formation factor from the approach described here. Other factors might include (1) using different data sets from different authors, (2) errors in the determination of the true in situ pore-fluid conductivity, and (3) possible incomplete saturation of some samples. Given these uncertainties, we feel that the excellent fit of a large data set to a single value of l with a high coefficient of correlation (0.911) for the relationship between σ_{surf}^{0} and σ'' suggests the use of a linear relation with a fixed l is appropriate. This approach provides strong opportunities to improve estimation of formation factor and salinity from single frequency measurements, as we have shown.

The experimentally determined value of l is generally consistent with the recently proposed mechanistic POLARIS model (Revil, 2012). Although we were unable to calculate l from the POLARIS model as estimates of the excess surface charge (Q_v) were unavailable in this database, the value of the partition coefficient f inferred from our experimental data is consistent with expected values assumed in the POLARIS model. However, this prediction (and by inference the performance of the POLARIS model) is highly dependent on the assumed ratio of the mobility of the ions in the Stern layer ($\beta_{\delta Þ Þ}^{S}$) to the mobility of the ions in the diffuse layer ($\beta_{\delta Þ Þ}$). This value is inherently uncertain, with some recent papers assuming that $\beta_{\delta Þ Þ}^{S}/\beta_{\delta Þ Þ}$ ¼ 1 (Revil and Florsch, 2010) and others suggesting that $\beta_{\delta Þ Þ}^{S}/\beta_{\delta Þ Þ}$ ¼ 0.0029 (Revil, 2012). Considering equation 16, changes in the ratio $\beta_{\delta Þ Þ}^{S}/\beta_{\delta Þ Þ}$ can be compensated by variations in the partition coefficient ratio $f/\delta 1 - f Þ$. For example, assuming $\beta_{\delta Þ Þ}^{S}/\beta_{\delta Þ Þ}$ ¼ 0.02 for our data set, the resulting partition coefficient f varies between 0.48 and 0.91 with a mean value of 0.75. This uncertainty in f and $\beta_{\delta Þ Þ}^{S}/\beta_{\delta Þ Þ}$ is only removed when one of the two quantities is reliably determined by experiments.

Knowledge of a well-constrained estimate of l provides opportunities for improved estimation of petrophysical properties from

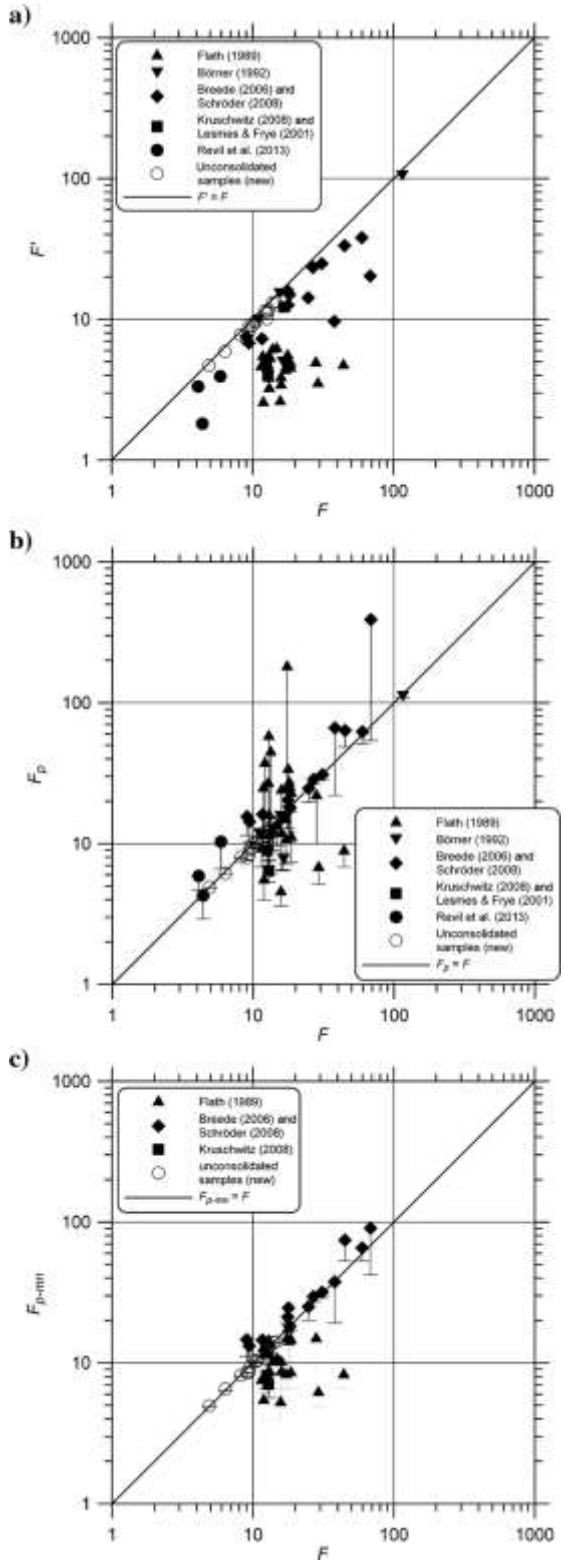

Figure 6. Crossplots of F versus F^0 estimated for a single salinity electrical measurement at 100 mS/m (Figure 6a), F versus F_p (Figure 6b), and F versus F_{p-mn} (Figure 6c) considering σ'' or m_n from an IP measurement and an assumed single value of l ¼0.042 or l_{mn} ¼0.20. The error bars indicate a variation of l between 0.042 and 0.064 (Figure 6b) and of l_{mn} between 0.20 and 0.30 (Figure 6c), respectively.

complex conductivity, i.e., by combining resistivity and IP measurements. We have demonstrated the potential value of this knowledge by showing the improvement of the estimation of true formation factor or salinity that can be obtained by using the imaginary conductivity and l to estimate σ^0_{surf} and thereby better resolve the electrolytic conductivity (σ_{el}) contribution to the measured real conductivity (σ^0). Examples of the approach for improving estimates of (1) F using a single known salinity and (2) σ_w when F is known (or assumed) have been demonstrated by comparing predictions against known values obtained when the IP measurement is used versus when it is not. In both cases, the addition of the IP measurement significantly improves the prediction, although scatter remains. This scatter is in part likely associated with variations in the value of l between samples (Figure 3). The estimation of F and σ_w appears improved when using the l_{mn} derived from the relationship between m_n (in place of σ'') and σ^0_{surf}, although this approach requires SIP data sets that may not always be available. For example, SIP data sets are still relatively rarely available in the field.

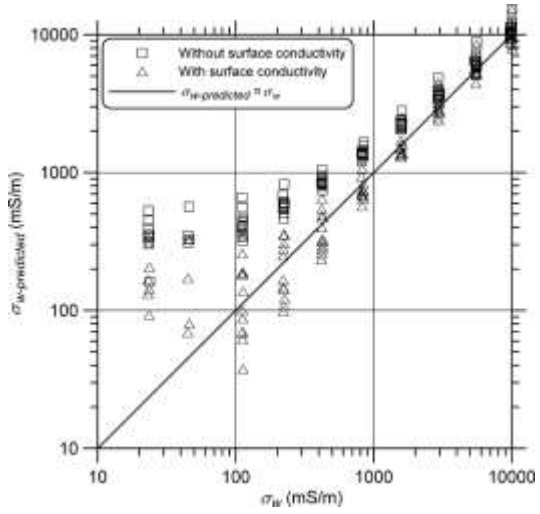

Figure 7. Fluid conductivity (σ_w) determined using equation 21 when (1) IP measurements were unavailable and surface conductivity was assumed to be negligible (i.e., $\sigma'' = 0$) and (2) when surface conductivity was estimated from σ'' and an assumed value of l (again set to 0.042). The solid line shows the true value of σ_w.

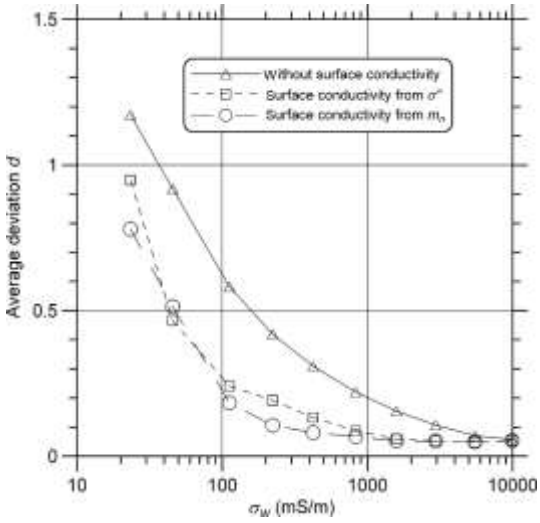

Figure 8. Average deviation d, which is determined by equation 23, between measured water conductivity (σ_w) and predicted water conductivity when (1) IP measurements were unavailable and surface conductivity was assumed to be negligible (i.e., $\sigma'' = 0$), (2) when surface conductivity was estimated from σ'' with an assumed value of $l = 0.042$, and (3) when surface conductivity was estimated from m_n with an assumed value of $l_{mn} = 0.20$.

The results of this research have potentially broad implications in well logging, in addition to surface geophysical surveys. In well logging, measurement of the formation factor is often required to determine porosity. The approach often requires an assumption that the salinity is high enough that the surface conductivity can be ignored, such that F can be estimated from a resistivity method and an estimate of the salinity of the formation water. Our findings suggest that well logging could be improved by inclusion of an IP measurement to constrain the surface conductivity. Currently, IP measurements are rarely used in well logging, except for exploration of ore minerals. In the emerging field of hydrogeophysics, resistivity methods are increasingly used to noninvasively monitor changes in electrolyte concentrations caused by contaminant transport, remediation strategies, groundwater-surface water exchange and aquifer storage and recovery. The transformation of resistivity changes into inferred changes in electrolyte concentrations typically requires an assumption that the surface conductivity can be ignored or be considered constant. The inclusion of IP measurements in hydrogeophysical monitoring could remove such dubious assumptions. The identification of a strong linear relationship between the imaginary conductivity and the real part of the surface conductivity provides the critical information needed to facilitate such an approach.

CONCLUSIONS

Using a large database composed of 63 samples in which complex conductivity was measured as a function of salinity, the relationship between the imaginary conductivity and the surface conductivity has been experimentally derived. This data set composed of sandstones and unconsolidated sediments satisfies a single linear relationship $\sigma'' = l \times \sigma^0_{surf}$ where $l = 0.042$ with a standard deviation of 0.022 (σ'' at 1 Hz, $R^2 = 0.911$). A similar strong relationship was found when the normalized chargeability determined from a DD model of the frequency dependence of the IP response was used in place of the single frequency imaginary conductivity. The surface conductivity is not salinity independent as is often assumed. Instead, the salinity dependence of the surface conductivity generally mimics that of the imaginary conductivity, showing evidence of an asymptotic approach to a high salinity maximum. We have demonstrated how our estimate of l can be used in conjunction with an IP measurement to improve petrophysical interpretation from resistivity and IP measurements, leading to improved prediction of the formation factor or water salinity. The relationship identified here has broad implications in well logging and in hydrogeophysics.

REFERENCES

Börner, F. D., 1992, Complex conductivity measurements of reservoir properties, *in* P. F. Worthington, and C. Chardaire-Rivière, eds., Advances in core evaluation: Reservoir management: Reviewed Proceedings of the Society for Core Analysis Third European Core Analysis Symposium, Harwood Academic, 359-386.

Börner, F. D., J. R. Schopper, and A. Weller, 1996, Evaluation of transport and storage properties in the soil and groundwater zone from induced polarization measurements: Geophysical Prospecting, 44, 583-601, doi: 10.1111/j.1365-2478.1996.tb00167.x.

Breede, K., 2006, SIP-Messungen an Sandsteinen: Unpublished diploma thesis, Technische Universität Clausthal.

Dukhin, S. S., and V. N. Shilov, 2002, Nonequilibrium electric surface phenomena and extended electrokinetic characterization of particles, *in* A. V. Delgado, ed., Interfacial electrokinetics and electrophoresis: Surfactant Science Series, 106, Marcel Dekker, 55-85.

Flath, D., 1989, The low-frequency complex electrical response of brine-saturated shaly sandstones: Unpublished Ph.D. thesis, University of Birmingham.

Kruschwitz, S., 2008, Assessment of the complex resistivity behavior of salt affected building materials: BAM-Dissertationsreihe, 30, Bundesanstalt für Materialforschung und -prüfung.

Leroy, P., and A. Revil, 2004, A triple layer model of the surface electrochemical properties of clay minerals: Journal of Colloid and Interface Science, 270, 371-380, doi: 10.1016/j.jcis.2003.08.007.

Leroy, P., and A. Revil, 2009, A mechanistic model for the spectral induced polarization of clay materials: Journal of Geophysical Research, 114, B10202, doi: 10.1029/2008JB006114.

Lesmes, D. P., and K. M. Frye, 2001, Influence of pore fluid chemistry on the complex conductivity and induced polarization responses of Berea sandstone: Journal of Geophysical Research, 106, 4079-4090, doi: 10.1029/2000JB900392.

Nordsiek, S., and A. Weller, 2008, A new approach to fitting induced-polarization spectra: Geophysics, 73, no. 6, F235-F245, doi: 10.1190/1.2987412.

Revil, A., 2012, Spectral induced polarization of shaly sands: Influence of the electrical double layer: Water Resources Research, 48, W02517, doi: 10.1029/2011WR011260.

Revil, A., and N. Florsch, 2010, Determination of permeability from spectral induced polarization in granular media: Geophysical Journal International, 181, 1480-1498, doi: 10.1111/j.1365-246X.2010.04573.x.

Revil, A., and P. W. J. Glover, 1997, Theory of ionic surface electrical conduction in porous media: Physical Review B, 55, no. 3, 1757-1773, doi: 10.1103/PhysRevB.55.1757.

Revil, A., and M. Skold, 2011, Salinity dependence of spectral induced polarization in sands and sandstones: Geophysical Journal International, 187, 813-824, doi: 10.1111/j.1365-246X.2011.05181.x.

Revil, A., M. Skold, S. S. Hubbard, Y. Wu, D. B. Watson, and M. Karaoulis, 2013, Petrophysical properties of saprolites from the Oak Ridge Integrated Field Research Challenge site, Tennessee: Geophysics, 78, no. 1, D21-D40, doi: 10.1190/geo2012-0176.1.

Rink, M., and J. R. Schopper, 1974, Interface conductivity and its implication to electric logging: Presented at Transactions of the SPWLA 15th Annual Logging Symposium, Paper J.

Schröder, H., 2008, SIP-Messungen an mit unterschiedlichen Salzlösungen gesättigten Sandsteinen: Unpublished diploma thesis, Technische Universität Clausthal.

Skold, M., A. Revil, and P. Vaudelet, 2011, The pH dependence of spectral induced polarization of silica sands: Experiment and modeling: Geophysical Research Letters, 38, L12304, doi: 10.1029/2011GL047748.

Slater, L., and D. P. Lesmes, 2002, Electrical-hydraulic relationships observed for unconsolidated sediments: Water Resources Research, 38, 1213, doi: 10.1029/2001WR001075.

Sumner, J. S., 1976, Principles of induced polarization for geophysical exploration: Elsevier.

Vinegar, H. J., and M. H. Waxman, 1984, Induced polarization of shaly sands: Geophysics, 49, 1267-1287, doi: 10.1190/1.1441755.

Waxman, M. H., and L. J. M. Smits, 1968, Electrical conductivities in oil-bearing shaly sands: SPE Journal, 243, 107-122, doi: 10.2118/1863-A.

Weller, A., K. Breede, L. Slater, and S. Nordsiek, 2011, Effect of changing water salinity on complex conductivity spectra of sandstones: Geophysics, 76, no. 5, F315-F327, doi: 10.1190/geo2011-0072.1.

Weller, A., and L. Slater, 2012, Salinity dependence of complex conductivity of unconsolidated and consolidated materials: Comparisons with electrical double layer models: Geophysics, 77, no. 5, D185-D198, doi: 10.1190/geo2012-0030.1.

Weller, A., L. Slater, S. Nordsiek, and D. Ntarlagiannis, 2010, On the estimation of specific surface per unit pore volume from induced polarization: A robust empirical relation fits multiple data sets: Geophysics, 75, no. 4, WA105-WA112, doi: 10.1190/1.3471577.